Supporting Information

Multifunctional Sulfamic Acid Additive for Synergistic Electrolyte Regulation toward Long-Cycling Aqueous Zinc-Ion Batteries

Zeqi Liu [a], Guopei Qiu [a], Kaihuan Liu [a], Wentao Li [a], Xinruo Xie [a], Yixin Zhou [a], Aokui Sun [a,b,*]

a School of Materials Science and Engineering, Hunan University of Technology, Zhuzhou 412007, China

b National & Local Joint Engineering Research Center for Advanced Packaging Material and Technology, Hunan University of Technology, Zhuzhou 412007, China

E-mail: aksun@hut.edu.cn

Address: No. 88, Taishan West Rd, Zhuzhou 412007, Hunan, China

S1 Experimental Section/Methods

S1.1 Preparation of VO_2

1.2 g V_2O_5 (Aladdin, 99%) and 1.8 g $H_2C_2O_4 \cdot 2H_2O$ (RHAWN, 99.5%) were dissolved in 40 mL deionized water. The solution was heated to 75℃ with magnetic stirring for 60 min to form a dark blue dispersion, which was then transferred into a 50 mL polytetrafluoroethylene (PTFE)-lined autoclave and held at 180℃ for 3 h. Finally, the product was washed three times sequentially with ethanol, deionized water, and ethanol, followed by vacuum drying at 60℃ for 12 h to yield VO_2(B). This synthesis protocol refers to previous literature [1].

S1.2 Material characterization

X-ray diffraction (XRD) patterns were acquired using a Rigaku SmartLab SE diffractometer (Japan). Contact angles were measured with a CA 100B goniometer. Fourier transform infrared (FTIR) spectroscopy (Nicolet 6700, 4000–500 cm^{-1}) and liquid nuclear magnetic resonance (NMR) spectroscopy (Bruker SU-8010, Germany, equipped with a coaxial NMR tube) were employed to investigate the effect of SA on water in the electrolyte. Raman spectroscopy (Horiba Lab-RAM HR Evolution) was used to analyze hydrogen bond content and SA coordination behavior. The morphology

of zinc foils was characterized by X-ray photoelectron spectroscopy (XPS, Nexsa), scanning electron microscopy (SEM, ZEISS Sigma 300, Germany), and atomic force microscopy (AFM, Bruker Dimension Icon), with AFM used to measure the roughness of cycled zinc foils. in-situ optical microscope(Murzider), to monitor the zinc deposition behavior in real time. Vanadium content in the electrolyte was determined via inductively coupled plasma mass spectrometry (ICP-MS, Thermo Scientific) to evaluate cathode dissolution.

S1.3 Electrochemical characterization

Cyclic voltammetry (CV), linear sweep voltammetry (LSV), chronoamperometry (CA), Tafel polarization tests, and electrochemical impedance spectroscopy (EIS, including charge transfer resistance characterization) were all performed on an Autolab electrochemical workstation. Specifically, LSV, CA, and Tafel tests were conducted using a three-electrode system (zinc foil as working electrode, platinum sheet as counter electrode, and Ag/AgCl as reference electrode); CV tests were carried out on Zn//VO_2 full cells; EIS measurements were performed on Zn//Zn symmetric cells and stainless steel (SS//SS symmetric cells), with a test frequency range of 0.01 Hz to 100000 Hz.

(i) The ionic conductivity

The ionic conductivity was obtained by testing the resistance of SS//SS symmetric cells and calculated using the following equation:

$$\sigma = L/(R_0 S) \tag{S1}$$

Where L denotes the electrolyte thickness (675μm), S is the surface area of the stainless steel with a diameter of 15 mm, and R_0 is the resistance determined via EIS measurements [2].

(ii) The Zn^{2+} transference number

I-t tests (polarization voltage: 10 mV; polarization time: 4,000 s) and EIS measurements (frequency range: 0.01 Hz to 10,0000 Hz, both before and after polarization) were performed on Zn//Zn

symmetric cells using an electrochemical workstation (CHI-660E). The Zn^{2+} transference number was calculated using Equation (2). A higher transference number indicates a greater proportion of Zn^{2+} in total charge transfer [3, 4].

$$t_{Zn^{2+}} = \frac{I_{ss}R_{\Omega,ss}\left(\Delta V - I_0 R_{ct,0}\right)}{I_0 R_{\Omega,0}\left(\Delta V - I_{ss}R_{ct,ss}\right)} \quad \text{(S2)}$$

In polarization measurements, I_0 represents the initial state current, while Is denotes the steady state current. The resistance values R_0 and Rs are obtained from EIS measurements conducted before and after polarization, respectively. The applied polarization potential is denoted as ΔV (10 mV).

S1.4 Constrained Peak Fitting for Raman Spectra (2800−3800 cm^{-1})

(1) The peak positions of the three sub-peaks (O-H1 ~3230.2 cm^{-1}, O-H2 ~3417.9 cm^{-1}, O-H3 ~3552.7 cm^{-1}) were allowed to vary within physically reasonable ranges, corresponding to the characteristic regions of strongly, moderately, and weakly hydrogen-bonded water, respectively; (2) A reasonable range (40-180 cm^{-1}) was set for the full width at half-maximum (FWHM) of each peak; (3) Iterative fitting was performed until χ^2 was minimized and the residuals showed a random distribution; (4) The coefficient of determination (R^2) for all fitted spectra exceeded 0.995. [5, 6]

We affirm that all compared electrolyte systems were processed using identical initial parameters and fitting procedures, ensuring the comparability of the results.

S1.5 XPS Peak Fitting

X-ray photoelectron spectroscopy (XPS) analysis was performed on a Thermo K-Alpha spectrometer using monochromatic Al Kα radiation (1486.6 eV). The spectra were directly acquired on the as-received surfaces without sputtering to avoid sputter-induced chemical changes. Binding energies were calibrated using the adventitious carbon C1s peak at 284.8 eV. Peak fitting was carried out using Avantage software. The binding energy ranges for peak fitting were constrained based on measured

values and literature references: for N 1s, 399.8–400.8 eV (adsorbed N species) and 401.6–402.6 eV (Zn_xNO_γ); for C 1s, 284.8 eV (fixed, adventitious carbon), 285.5–286.5 eV (C–O/C–N), and 288.4–289.4 eV (carbonate); for S 2p, 163.1–164.1 eV (ZnS), 168.7–169.7 eV ($ZnSO_3$), and 170.0–171.0 eV (sulfate). The S2p spin–orbit splitting was fixed at 1.18 eV with an area ratio of 2:1. All peaks were fitted using a Shirley background and a Gaussian–Lorentzian (GL 30) line shape, with FWHM constrained within 1.2–2.0 eV [7-9]. The fitting conditions were kept strictly consistent for both the control and experimental groups to ensure comparability of results.

S1.6 Concentration screening table

Table S1. Comparison of multi-parameter performance of electrolytes with different SA concentrations

SA concentration (mM)	Ionic conductivity (mS cm^{-1})	pH	Corrosion potential (V)	Corrosion current density(mA cm^{-2})	Cycle life of Zn//Zn cell (h, at 1 mA cm^{-2}/ 1 mAh cm^{-2})
0	3.71	4.08	-0.985	0.9812	60
10	5.75	2.67	-0.982	0.9586	230
12	**10.03**	**2.54**	**-0.974**	**0.363**	**3228**
15	10.55	2.35	-0.969	0.4116	880
20	8.23	2.17	-0.975	0.3178	510
30	4.54	1.93	-0.975	0.51	421

S2 Supplementary Figures

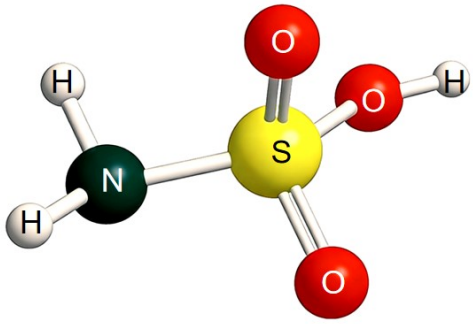

Fig. S1. Molecular structure of sulfamic acid

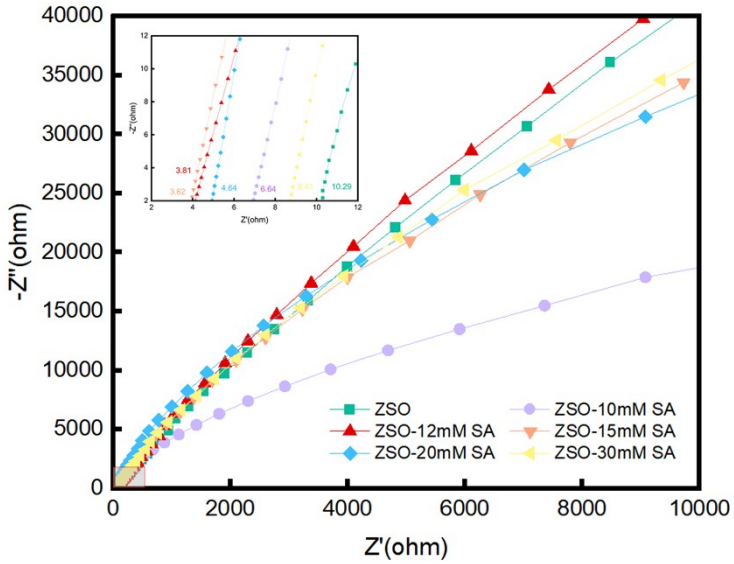

Fig. S2. Bulk impedance of electrolytes with different additive concentrations

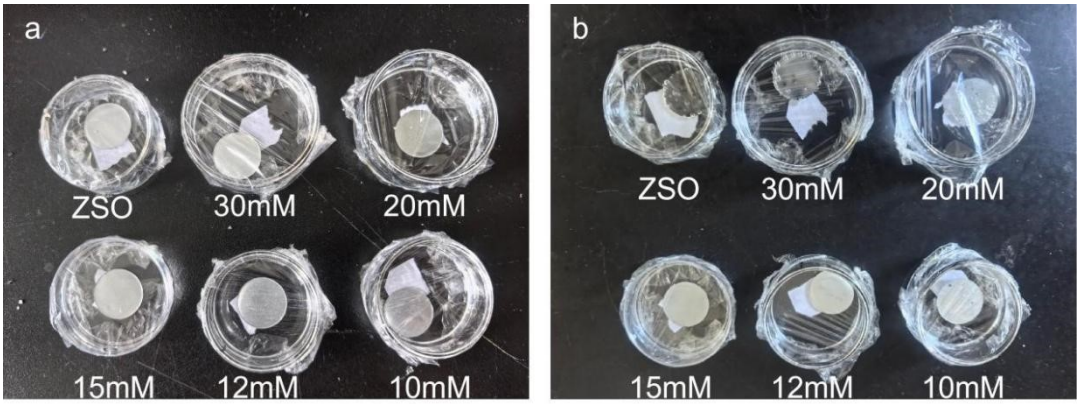

Fig.S3. Optical images of zinc foils soaked in electrolytes with varying additive concentrations: (a) 0 days soaking, (b) 5 days soaking

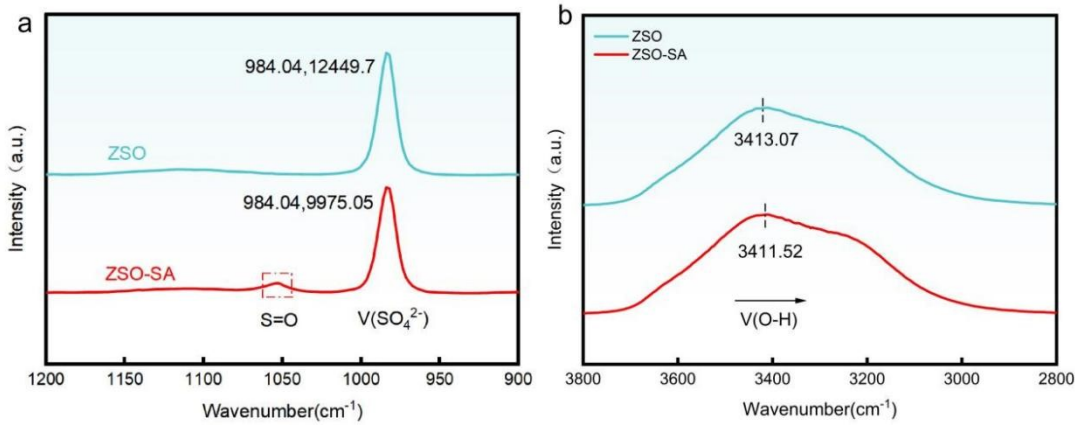

Fig. S4. Raman spectra of different electrolytes: (a) 900–1200 cm^{-1}, (b) 2800–3800 cm^{-1}

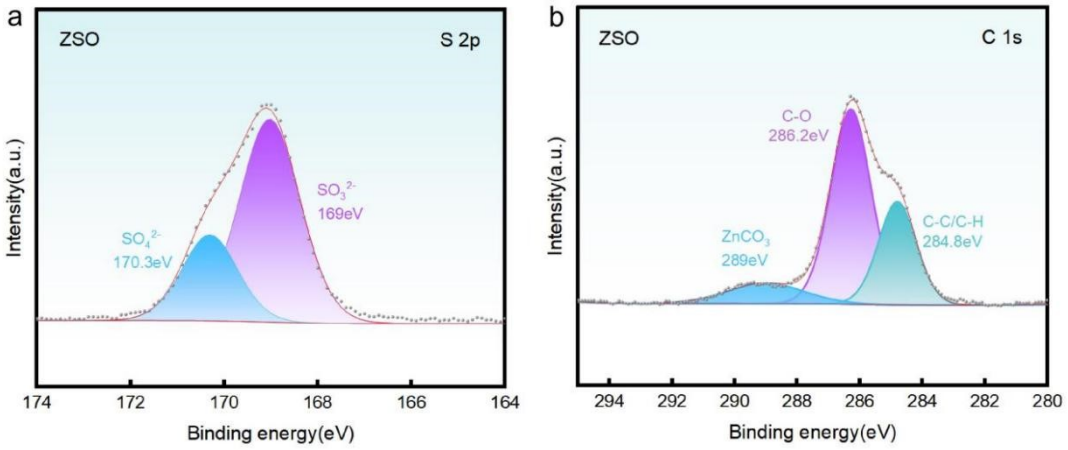

Fig. S5. XPS spectra of the zinc anode surface after 150 h cycling in ZSO electrolyte: (a) S2p, (b) C1s

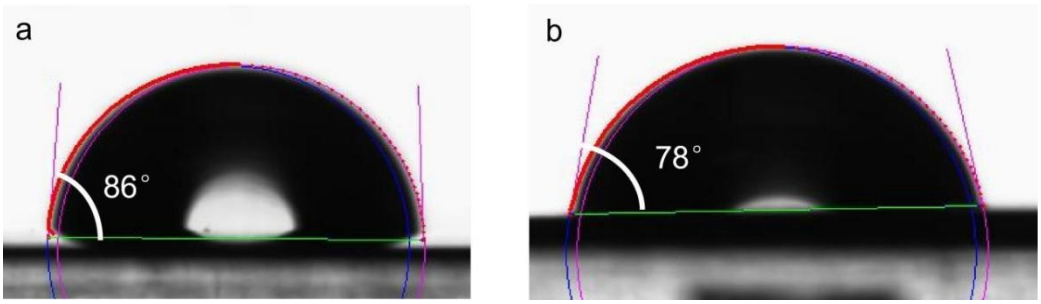

Fig. S6. Contact angles of deionized water on zinc foils after 150 h cycling in different electrolytes: (a) ZSO-SA electrolyte, (b)

ZSO electrolyte

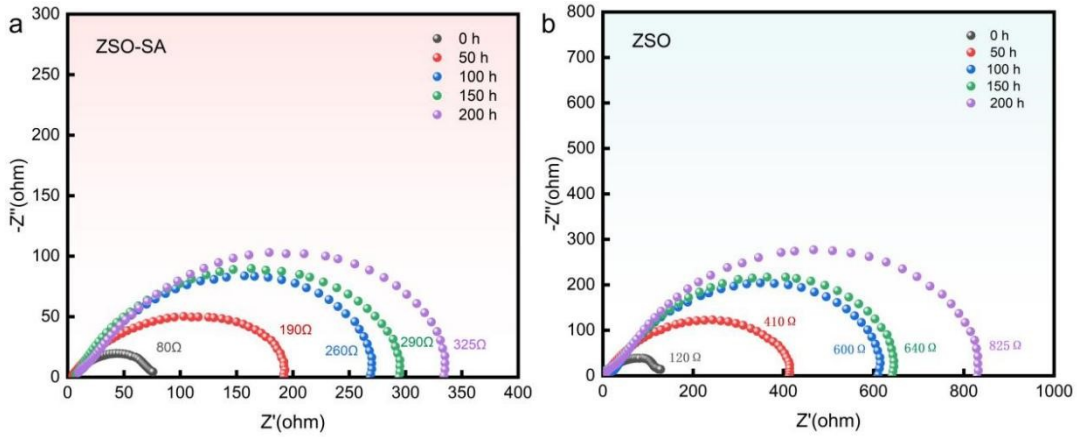

Fig. S7. EIS plots of Zn//Zn symmetric cells with different electrolytes after different cycling times at 1 mA cm^{-2}/1 mAh cm^{-2}: (a)

ZSO-SA electrolyte, (b) ZSO electrolyteelectrolyte

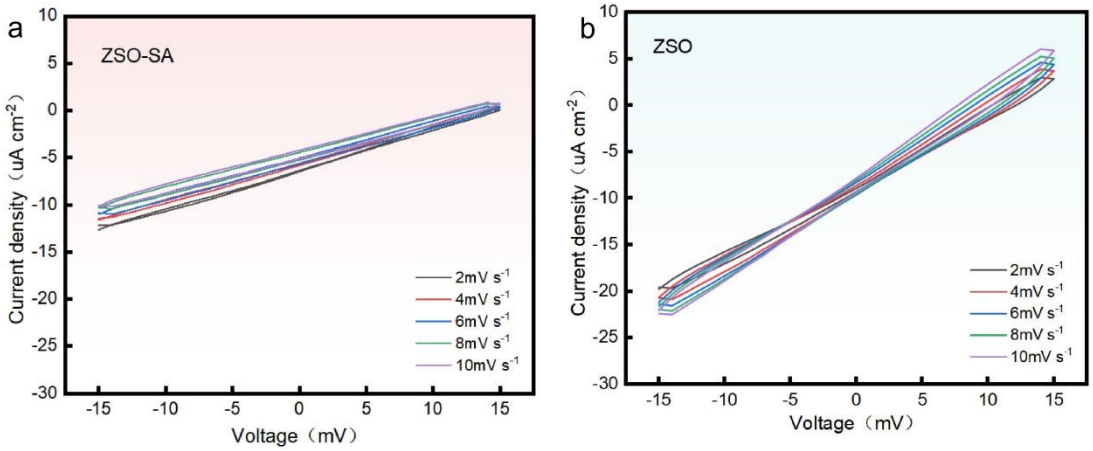

Fig. S8. CV tests of Zn//Zn symmetric cells at different scan rates with a voltage range of −15 mV to 15 mV (vs. Zn/Zn^{2+}): (a) ZSO-SA electrolyte, (b) ZSO electrolyte

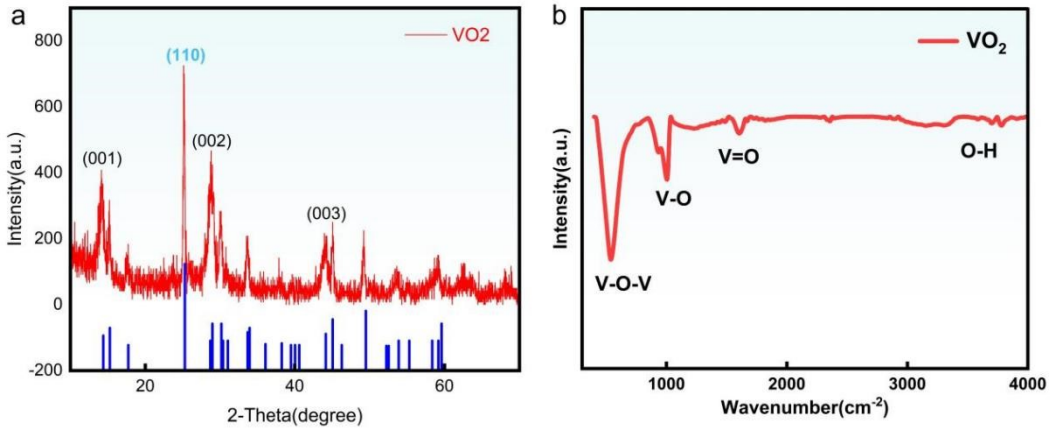

Fig. S9. (a) XRD and (b) FTIR spectra of hydrothermally synthesized VO_2 powder

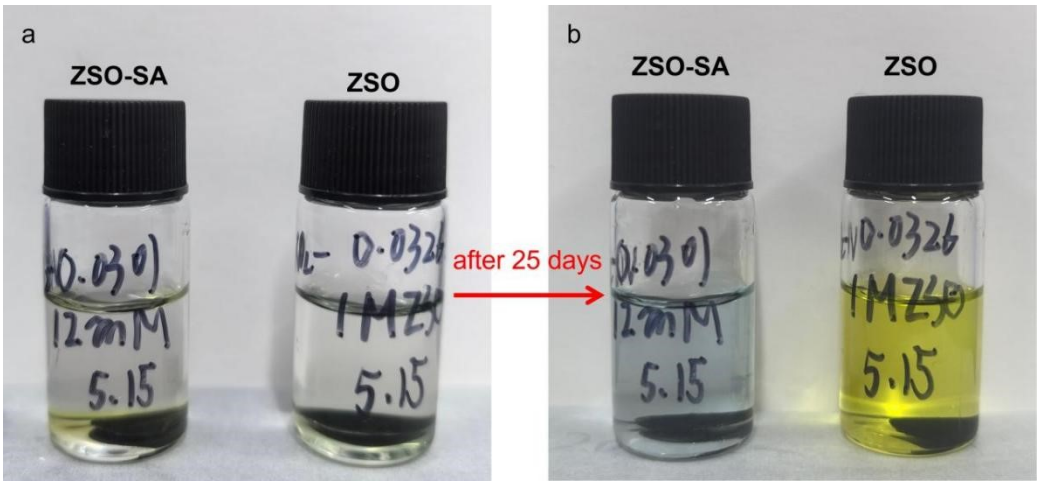

Fig. S10. Optical images of VO_2 cathode sheets soaked in electrolytes with/without SA additive: (a) 0 days, (b) 25 days

References

[1]Zhang Y, Wang R, Ao H, et al. Zn^{2+}-rich chelate layer facilitates ultrahigh-rate zinc anodes via cation compensation and anion repulsion. Advanced Energy Materials, 2025, 15(18): 2404203.

[2]Zheng G, Yan T, Hong Y, et al. A non-newtonian fluid quasi-solid electrolyte designed for long life and high safety Li-O_2 batteries. Nature Communications, 2023, 14(1): 2268.

[3]Zeng W, Wang X, Huang Y, et al. Multi-functional additive to enhance cycling performance of Zn anode in aqueous battery. Journal of Power Sources, 2024, 595: 234075.

[4]Yin J, Li M, Feng X, et al. Unveiling the multifunctional regulation effect of a glutamine additive for highly reversible Zn metal anodes. Journal of Materials Chemistry A, 2024, 12(3): 1543-1550.

[5]Liu T, Lei C, Wang H, et al. Aqueous electrolyte with weak hydrogen bonds for four-electron zinc–iodine battery operates in a wide temperature range. Advanced Materials, 2024, 36(32): 2405473.

[6]Zhang Q, Xia K, Ma Y, et al. Chaotropic anion and fast-kinetics cathode enabling low-temperature aqueous Zn batteries. ACS Energy Letters, 2021, 6(8): 2704-2712.

[7]Xu X, Su H, Zhang J, et al. Sulfamate-derived solid electrolyte interphase for reversible aqueous zinc battery. ACS Energy Letters, 2022, 7(12): 4459-4468.

[8]Wu J, Liu C, Zhang H, et al. Regulation of the electrochemical plating/stripping process for Zn: multifunctional effects of N, S-codoped carbon dots[J]. The Journal of Physical Chemistry Letters, 2022, 13(51): 11883-11891.

[9]Liu C, Xie D, Jiang W B, et al. Proton-driven bilateral interfacial chemistry and electrolyte structure reconstruction enable highly reversible zinc metal anodes. Energy Storage Materials, 2024, 70: 103497.